Title

Autism spectrum disorder risk genes have convergent effects on transcription and neuronal firing patterns in primary neurons

Running Title

ASD genes effect transcription and neuron firing

Authors

Alekh Paranjapye[1,#], RIli Ahmad[1,#], Steven Su[1], Abraham J. Waldman[3], Jennifer Philips-Cremins[1,2,3], Shuo Zhang[2], Erica Korb[1,2,*]

Affiliations

[1]Department of Genetics, Perelman School of Medicine, [2]Epigenetics Institute, Perelman School of Medicine, University of Pennsylvania Perelman School of Medicine, [3]Department of Engineering, School of Engineering and Applied Science, University of Pennsylvania, Philadelphia, PA, USA

# indicates equal contribution

*corresponding author: Erica Korb, ekorb@pennmedicine.upenn.edu

Abstract

Autism spectrum disorder (ASD) is a highly heterogenous neurodevelopmental disorder with numerous genetic risk factors. Notably, a disproportionate number of risk genes encode transcription regulators including transcription factors and proteins that regulate chromatin. Here, we tested the function of nine such ASD-linked transcription regulators by depleting them in primary cultured neurons. We then defined the resulting gene expression disruptions using RNA-sequencing and tested effects on neuronal firing using multielectrode array recordings. We identified shared gene expression signatures across many ASD risk genes that converged on disruption of critical synaptic genes. Fitting with this, we detected drastic disruptions to neuronal firing throughout neuronal maturation. Together, these findings provide evidence that multiple ASD-linked transcriptional regulators disrupt transcription of synaptic genes and have convergent effects on neuronal firing that may contribute to enhanced ASD risk.

Introduction

Autism Spectrum Disorder (ASD) is a highly prevalent neurodevelopmental disorder with numerous risk genes (De Rubeis et al. 2014; Iossifov et al. 2014; Sullivan and Geschwind 2019; de la Torre-Ubieta et al. 2016). Major functional groups of ASD risk genes have emerged including a large portion that encode proteins that regulate transcription (Iossifov et al. 2014; O'Roak et al. 2012; Parikshak et al. 2013; De Rubeis et al. 2014). Of these ASD-linked transcriptional regulators, many encode proteins that regulate chromatin, the complex of DNA and histone proteins that helps to regulate transcription. Others encode transcription factors while still others directly modify DNA itself. Thus, distinct groups of proteins with disparate functions in transcriptional regulation can lead to overlapping phenotypic outcomes.

We previously tested the effects of disrupting a set of ASD risk genes that function as chromatin regulators and found that they affected expression of a common set of genes that

52 encode synaptic proteins (Thudium et al. 2022). This gene expression signature was detected in
53 multiple systems and, together with the broader literature (Satterstrom et al. 2020; Zhao et al.
54 2018), suggest that neurons have gene sets that are highly susceptible to chromatin disruptions
55 regardless of the specific manipulation with similar signatures found across other psychiatric
56 disorders (Rajarajan et al. 2018; Schrode et al. 2019). Further, numerous studies have identified
57 sets of synaptic genes that have unique chromatin features and that are disrupted in ASD, either
58 directly as ASD risk genes or indirectly following disruption of ASD-linked transcriptional
59 regulators (Satterstrom et al. 2020; Zhao et al. 2018). Both our work and others (Thudium et al.
60 2022; Satterstrom et al. 2020) found that the targets of ASD-linked transcriptional regulators do
61 not directly regulate other ASD-linked gene more than is expected by chance and instead target
62 synaptic genes more broadly. However, prior analysis was limited to a handful of chromatin
63 regulators. Whether similar transcriptional signatures are detected in response to disruption of
64 transcriptional regulators more broadly beyond just chromatin-modifying enzymes, and whether
65 such changes result in shared functional outcomes remain unclear.

66 To address these outstanding questions, we used a primary neuronal culture model to
67 allow for comparisons within a highly controlled, genetically identical population of neurons. We
68 partially depleted chromatin regulators, DNA modifying enzymes, and transcription factors that
69 are all strongly linked to ASD. Using RNA-sequencing, we defined gene expression signatures
70 common between these ASD-linked transcriptional regulators. We identified shared gene
71 expression signatures that encoded critical neuronal proteins including numerous synaptic
72 proteins. We next used multielectrode array (MEA) recording to test the functional implications
73 of these transcriptomic changes on neuronal firing patterns. Every transcriptional regulator
74 tested affecting spiking and bursting patterns throughout neuronal maturation. These data
75 demonstrate that disruption of multiple types of ASD-linked transcriptional regulators results in
76 shared gene expression signatures and neuronal firing patterns despite having divergent effects
77 on chromatin and gene regulation. Our findings define shared functional outcomes of distinct

ASD-linked genes during neuronal maturation, improving our understanding of the molecular basis for ASD and related neurodevelopmental disorders.

Results

Depletion of ASD-linked transcriptional regulators affects gene expression

Here, we sought to define shared gene expression signatures amongst multiple ASD-linked transcriptional regulators including *ASH1L, CHD8, DNMT3A, KDM6B, KMT2C, MBD5, MED13L, SETD5,* and *TBR1*. We selected these targets to jointly test the roles of chromatin regulators, DNA modifying enzymes, and transcription factors, expanding upon prior work that focused on single classes of these proteins. Importantly, we chose chromatin modifying enzymes that target different both distinct (*KDM6B, KMT2C)* and overlapping (*ASH1L, SETD5)* histone sites*,* histone remodelers from 2 different complexes (*CHD8, MED13L),* a DNA modifying enzyme *(DNMT3A*), a transcription factor (*TBR1*)*,* and a non-catalytic chromatin-complex protein (*MBD5*) (**Table 1**). Additional criteria included that each are high confidence ASD genes (score as a '1' within the SFARI gene module and are significant TADA genes), lead to well-defined syndromes or associated phenotypes caused by loss-of-function mutations or deletions, and have been successfully modeled in mice (Fu et al. 2022; Gao et al. 2021; Shen et al. 2019; Brauer et al. 2023; Lavery et al. 2020; Nakamura et al. 2024; Moore et al. 2019; Beighley et al. 2020; Bernier et al. 2014; Chatterjee et al. 2021; Hurley et al. 2021; Adegbola et al. 2015; Christian et al. 2020; Li et al.; Huang et al. 2019; Mullegama and Elsea 2016; Camarena et al. 2014).

Protein	Function	Target	SFARI Score	EAGLE Score	Associated Disorders	Mouse Phenotype?
ASH1L	Histone lysine methyltransferase	H3 Lysine 36	1	14.15	Emerging MCA/ID disorder	X
CHD8	Chromodomain helicase	Chromatin remodling	1	97.65	CHD8-NDD	X
DNMT3A	DNA methyltransferase	DNA	1	15.9	DNMT3A overgrowth syndrome	X
KDM6B	Histone demethylase	H3 Lysine 27	1	13.75	Stolerman neurodevelopmental syndrome	X
KMT2C	Histone lysine methyltransferase	H3 Lysine 4	1	-	Kleefstra syndrome	X
MBD5	Transcription regulator	Nonenzymatic histone regulator	1	46.6	MAND, 2q23.1 microdeletion syndrome	X
MED13L	Part of Mediator complex	RNA polymerase II transcribed genes	1	35	MRFACD syndrome	X
SETD5	Histone lysine methyltransferase	H3 Lysine 36	1	28.05		X
TBR1	Transcription factor	Developmental gene programs	1	-		X

Table 1: Function and association data for the nine transcriptional regulators chosen for analysis. SFARI gene score of 1 indicates high confidence for implication in autism spectrum disorder. Evaluation of Autism Gene Link Evidence (EAGLE) score ranges from 6 (limited) to 12+ (definitive) roles in autism for validated targets.

To test these genes of interest, we used primary neuronal cultures derived from E16.5 embryonic mouse cortical tissue to generate a highly pure neuron population (**Fig. 1A**) (Thudium et al. 2022). This allows for all targets to be tested within the same cell population without the complexity and heterogeneity of brain tissue. Further, this system provides a genetically identical background which avoids confounding variables from the mixed backgrounds from patient samples. This system is also sufficiently tractable to test multiple candidate genes in parallel within neurons derived from the same embryo, thus providing a highly controlled system for comparisons and true biological replicates. Lastly, this system allows for targeting of transcriptional regulators in neurons following isolation from tissue and establishment of neuronal identity. This ensures that the same cell types are measured across conditions by avoiding disruptions to neuronal precursor cells that ultimately might affect cell identity, or the ratio of inhibitory and excitatory neurons present during testing. While disruptions during early neurogenesis are almost certainly highly relevant to the biology underpinning ASD, here we specifically sought to focus on effects within post-mitotic neurons to allow for direct

115 comparisons in equivalent cell types without disrupted developmental trajectories. Together, this
116 system therefore allows for the parallel testing of multiple genes across multiple biological
117 replicates on a genetically identical background during a key period of neuronal maturation
118 without changes in cell identity.

119 We cultured neurons derived from 6 wildtype E16.5 cortices (3 male and 3 female) and
120 infected neurons with lentivirus containing shRNA at 5 days in vitro (DIV) to achieve partial
121 depletion of targets and model a partial loss of function variant. Depletion of each target
122 transcript was confirmed at DIV 10 (**Fig. S1A**) and, where antibodies were available, similarly
123 confirmed depletion at the protein level here (**Fig. S1B**) or in prior work (Thudium et al. 2022).
124 We then performed RNA-sequencing at DIV 10, the timepoint when we previously identified
125 robust transcriptional effects of multiple ASD-risk genes (Thudium et al. 2022). We again
126 confirmed knockdown of each target, and, similar to prior findings (Thudium et al. 2022),
127 determined that these transcriptional regulators do not directly affect gene expression of the
128 other ASD-linked transcriptional regulators examined here (**Fig. 1B**). This suggests that any
129 shared downstream effects are not simply due to one target causing disruption of another and
130 thus also disrupting their target genes indirectly.

131 Next, we defined differentially expressed genes (DEGs) following depletion for all targets
132 (**Fig. 1C, Supplemental Data Table 1**). Importantly, we did not detect any DEGs comparing
133 non-targeting shRNA viral infection controls to non-infected neurons indicating that the viral
134 infection alone did not perturb gene expression in neurons (**Fig. S1C-D**). All targeted shRNAs
135 caused gene expression changes, although to markedly differing degrees. Notably, the degree
136 of knockdown was not strongly correlated with the number of DEGs identified or the basal
137 expression level of the target itself (**Fig. S1E-F**). This suggests that some ASD-linked
138 transcriptional regulators have more robust effects on neurons during early maturation stages
139 than others due their functional relevance to transcription in this culture system rather than due
140 to technical factors. We performed gene ontology analysis on each group of significantly altered
141 genes and found a wide range of enriched molecular and biological pathways across DEGs by

142 depletion (Supplemental Data Table 2). These included dysregulations of genes associated with
143 immune functioning such as with *Tbr1, Ash1l*, and *Kmt2c* (Fig. 1D) as well as extracellular
144 components in *Kdm6b, Chd8*, and *Mbd5*. *Med13l* and *Chd8* loss resulted in the greatest total
145 number of differential expressed genes at this neuronal time point. *Med13l* depletion showed
146 strong enrichment in metabolism for upregulated genes and neuron functioning and
147 transmembrane transport genes for downregulated genes (Fig. 1E). These findings were
148 recapitulated using the synapse-specific gene ontology analysis SynGO (Fig. 1F). To determine
149 the extent to which each depletion affected synaptic functioning beyond the most significant
150 DEGs, we performed gene set enrichment analysis for each dataset examining expression
151 change trends for postsynaptic membrane potential and synapse adhesion (Fig. 1G-H). Nearly
152 every target showed significant downward trends for these key neuronal pathways. Notably,
153 while prior work found that these gene sets are highly sensitive to chromatin disruptions, these
154 analyses extend these findings to other forms of transcriptional regulation beyond histone
155 modifying enzymes. Together, this work demonstrates that a broad range of ASD-linked
156 transcriptional regulators serve to control expression of synaptic genes in immature neurons.
157
158

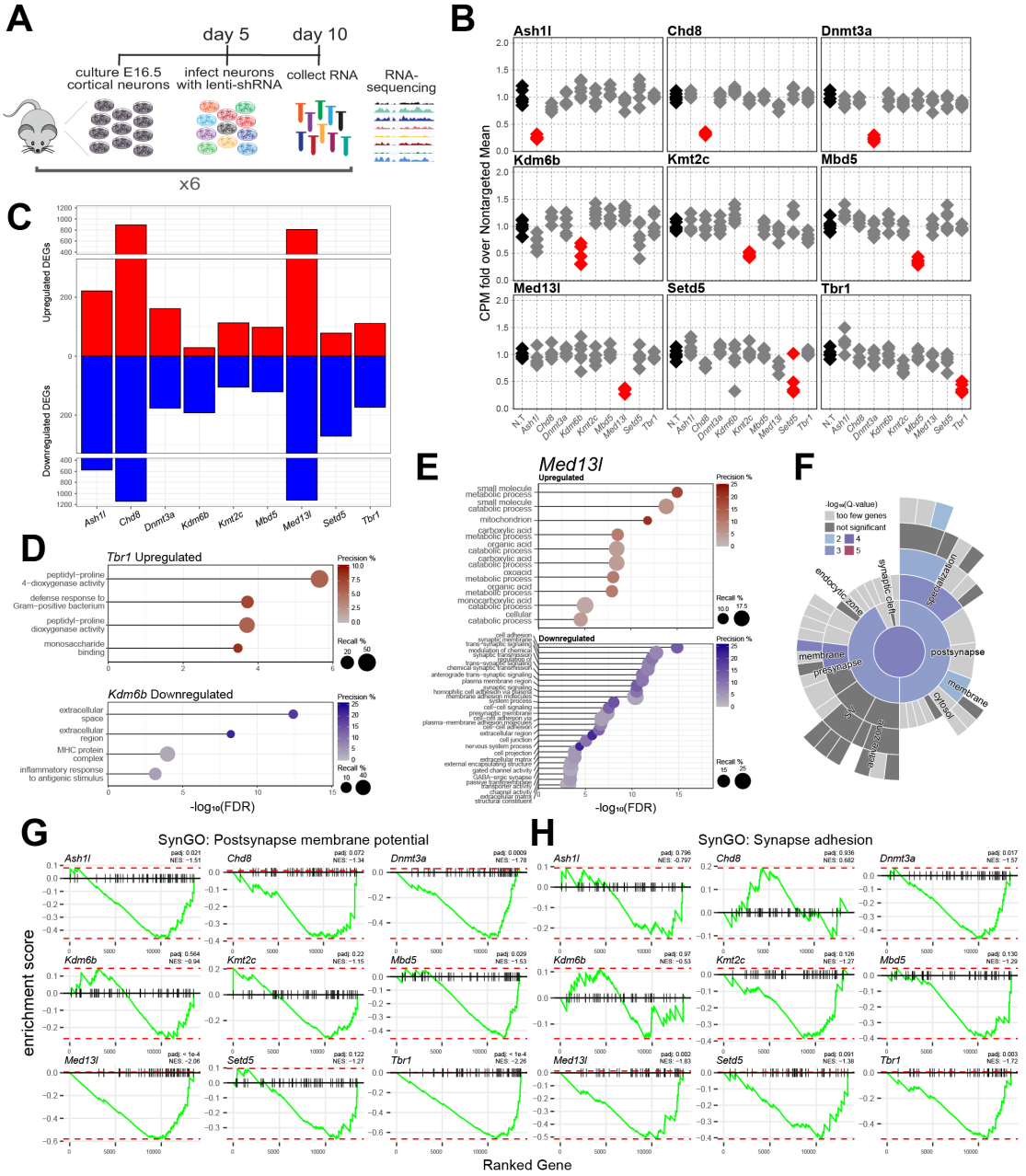

Figure 1: Gene expression analysis of nine independent chromatin modifier depletions in primary mouse neurons. A. Schematic of the experimental timeline for the comparison of transcriptomes between chromatin modifier depletions. B. Counts per million (CPM) for the nine chromatin modifiers following lentivirus-mediated shRNA depletion of each target, relative to the average of nontargeting (N.T.) treated neurons (n = 6). C. Total up or downregulated differentially expressed genes (DEGs) in the pairwise comparison of each depletion versus N.T. treated neurons. Full DEG lists shown in Supplemental Table 1. D-E. Gene ontology analysis of significantly up and downregulated genes in the depletion of Tbr1 or Kdm6b (D) and Med13l (E). Recall is the proportion of functionally annotated genes in the query over the number of genes in the GO term. Precision is the number of genes found in the GO term over the total number of genes in the query. Results for other targets shown in Supplemental Table 2. F. SynGO for Med13l significantly downregulated DEGs. G-H. GSEA of genes in the SynGO postsynaptic membrane potential (G) or synaptic adhesion (H) terms for each depletion transcriptional signature. NES indicates the directional normalized enrichment score.

160 **Depletion of ASD-linked transcriptional regulators cause shared gene expression**
161 **changes.**

162 Notably, each individual shRNAs can have off-target effects that may contribute to
163 transcriptional changes. Therefore, we sought to compare the effects of 9 different targets on
164 gene expression and focus on their shared transcriptomic outcomes. We anticipate that through
165 this approach, we are more likely to detect gene sets that are most sensitive to loss of ASD
166 linked genes rather than an off-target effect of a single shRNA. To define overlapping
167 transcriptional changes, we first directly compared DEGs from each target and found significant
168 overlap among many (**Fig. 2A-D, Supplemental Data Table 3**). This fits with prior results that
169 suggest that ASD-linked transcriptional regulators share multiple gene targets despite acting
170 through disparate mechanisms in chromatin (Thudium et al. 2022). Interestingly, we found little
171 overlap with high-confidence ASD risk genes (**Fig. S2A**). This supports prior findings (Thudium
172 et al. 2022) and suggests that ASD-linked transcriptional regulators cause neuronal disruption
173 through mechanisms distinct from simply directly dysregulating other ASD-linked synaptic
174 genes.

175 We next sought to identify functional enrichment in shared gene sets. We found that
176 genes that were differentially expressed in at least two or three gene sets encoded proteins
177 relevant to neuronal function such as transmembrane transporters and trans-synaptic signaling
178 components (**Fig. 2E**). Further, these genes shared several chromatin signatures (**Fig. S2B**).
179 Gene sets detected in at least 2 or 3 conditions were enriched for genomic regions that
180 contained bivalent domains similar to prior findings (Thudium et al. 2022). Interestingly, we also
181 found that down regulated genes typically having longer gene lengths (**Fig. 2F**). These findings
182 suggest that instances of specific genomic features (Zhao et al. 2018) and disrupted expression
183 of long genes (King et al. 2013) are common features of transcriptional disruptions underlying
184 ASD. Together, these findings indicate that ASD-linked transcriptional regulators share gene
185 targets, particularly long genes that may sensitize them to disruption, and have common
186 functional outcomes in regulating expression of genes that function at neuronal synapses.

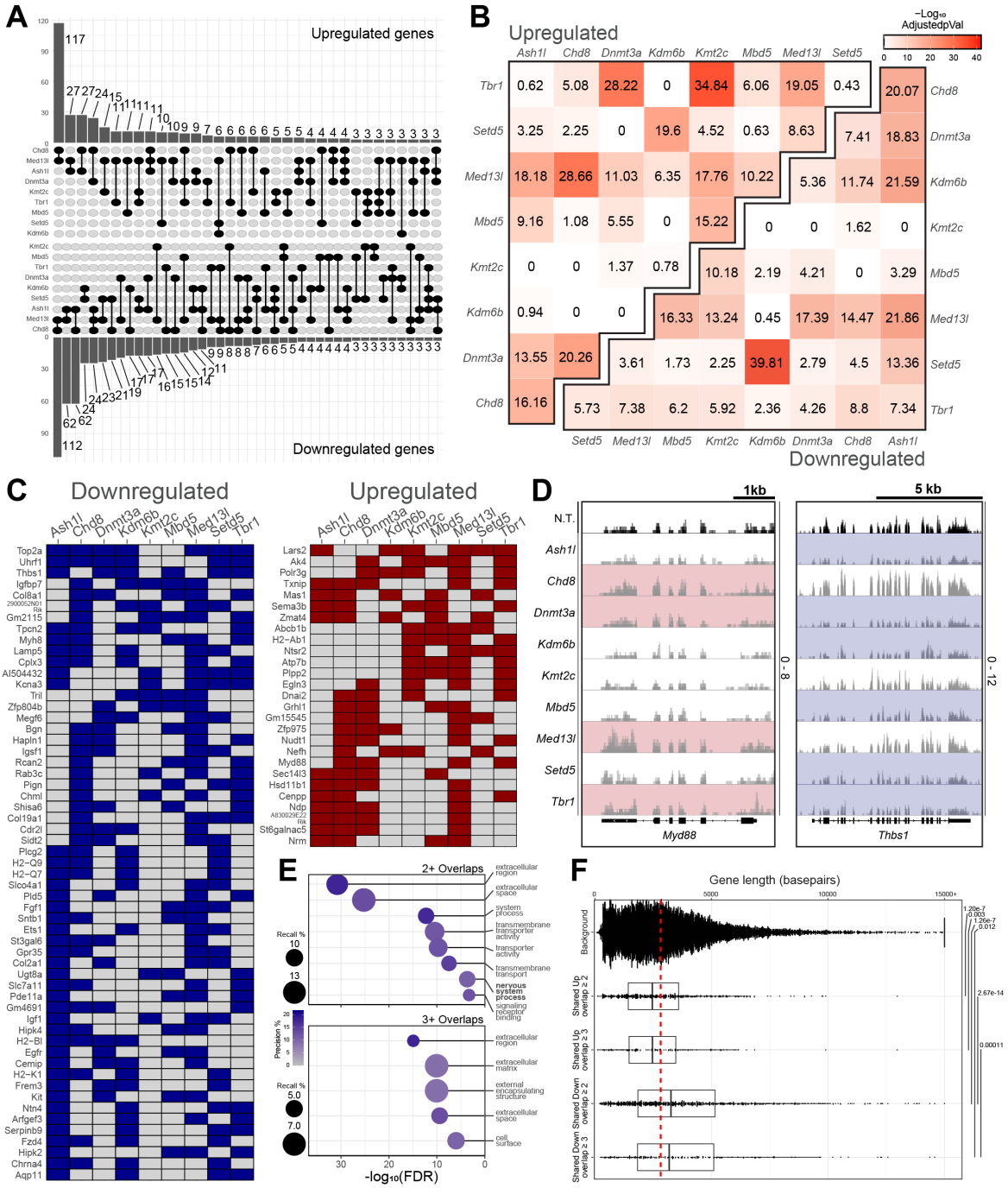

Figure 2: Identifying transcripts that co-dysregulated across depletions. A. Upset plot of up or downregulated DEG found in at least two depletions. Gene placement prioritizes the largest intersection possible, only showing overlaps with 3 or more DEGs. B. Significance of overlap for up or downregulated DEGs after each depletion using hypergeometric tests. C. Heatmap of DEGs that appear in 4+ (left, downregulated, right, upregulated) comparisons between depletion and N.T. control. D. Gene tracks of aligned transcripts over genes that were either upregulated (Myd88) or downregulated (Thbs1) in multiple depletions. E. Gene ontology analysis of all significantly downregulated genes found in over 2 or over 3 depletion conditions. F. Boxplots of the transcript lengths for all genes, each DEG found up or downregulated in at least 2 pairwise depletions, or 3 pairwise depletions. T-test p values for each pairwise comparison are noted on the side.

188 **Defining common transcriptional signatures ASD-linked transcriptional regulators.**

189

190 We next used limma-voom analysis (Law et al. 2014a; Ritchie et al. 2015) to generate a
191 differential gene expression model factoring all transcriptional regulators together to define
192 common transcriptional signatures that diverge from control infected neurons. We found that
193 this multi-condition modeling of the depletions together resulted in significant up and down
194 regulated gene sets with a greater number of downregulated genes identified (**Fig. 3A,**
195 **Supplemental Data Table 4**). To understand what combinations of transcriptional regulators
196 contributed to the transcriptional signature identified by limma, we examined top hits from this
197 analysis and found genes with similar changes in gene expression across multiple conditions
198 (**Fig. 3B-C**). As expected, this signature includes many of the DEGs found in at least 2 or 3
199 direct comparisons (**Fig. 3D**). Pairwise comparisons of the trends in gene expression of the
200 shared limma signature model showed variable but strong correlations and overlaps between
201 nearly every pair of targets indicating that this approach was successful in identifying
202 convergent gene sets that link all 9 targets (**Fig. 3E**).

203 We used gene ontology to examine the function of these gene sets and found that
204 upregulated genes were enriched for those with proteasomal and endopeptidase activity while
205 those that were downregulated were primarily trans-synaptic signaling similar to the previous
206 overlap analysis. (**Fig. 3F**). We observed a small but significant overlap between the
207 downregulated signature and ASD risk genes (**Fig. S3A**) and again found that downregulated
208 genes are longer than nondifferential expressed genes (**Fig. S3B**). Together, these findings
209 define a transcriptional signature that is shared across the target genes of multiple ASD-linked
210 transcriptional regulators. This signature expands upon prior work (Thudium et al. 2022)
211 demonstrating that long synaptic genes are highly sensitive to chromatin disruptions.
212 Importantly, these findings demonstrate such features are true of ASD-linked transcriptional
213 regulators more broadly than only ASD-linked chromatin modifying enzymes.

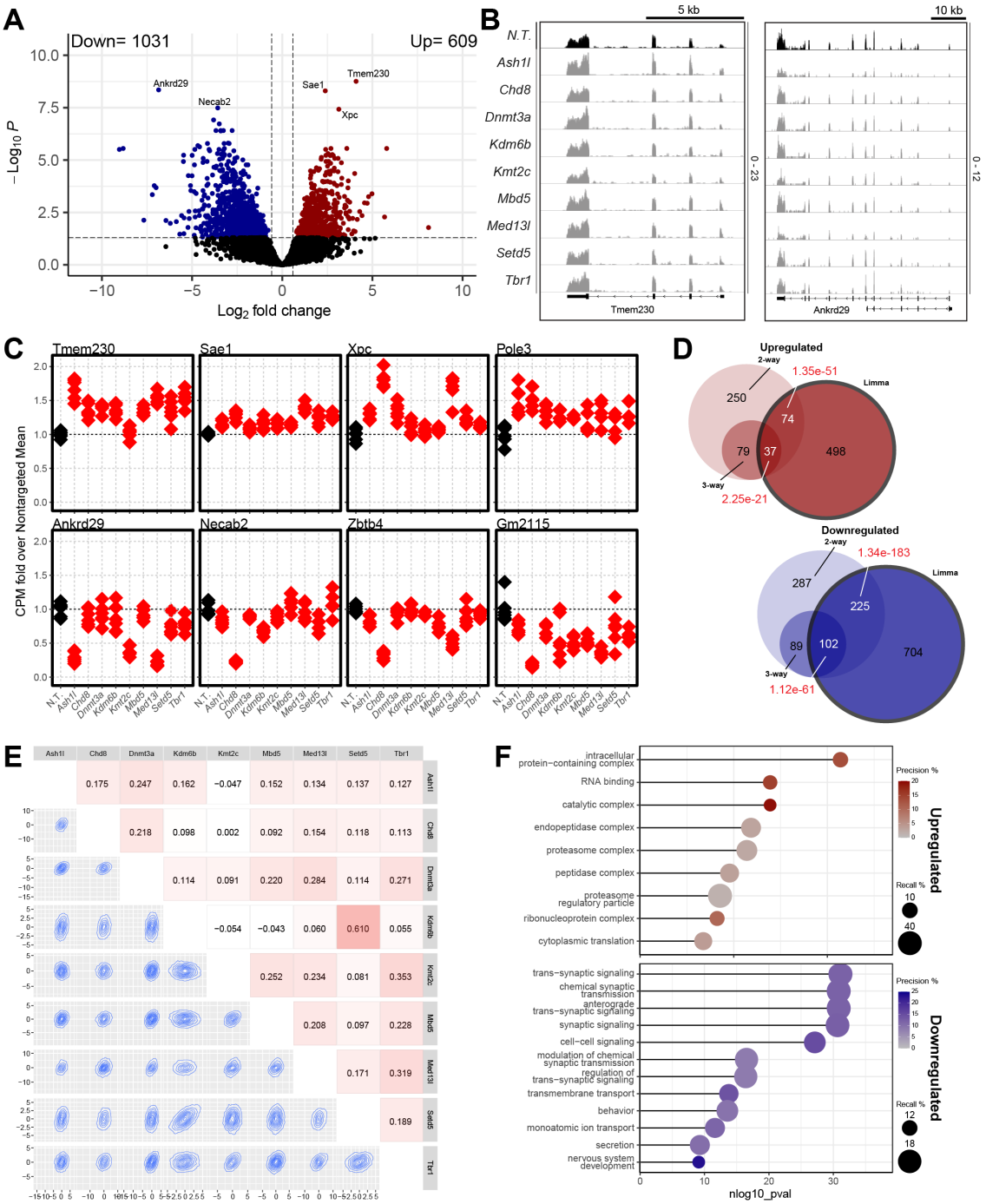

Figure 3: Multiple factor linear modeling to determine commonly disrupted transcripts across all nine depletions. A. Volcano plot of DEGs from the limma/voom model factoring all nine depletion conditions against N.T. control. B. Gene tracks of transcripts of the top 2 DEGs Tmem230 and Ankrd29. C. Relative expression of the top DEGs identified in the multi-factor model in each depletion versus the average of nontargeting (N.T.) treated neurons. D. Overlap of genes down or upregulated in at least 2 (i) or 3 (ii) pairwise comparisons and those from the multi-factor model. Hypergeometric test results for each overlap as shown in red. E. Cross-correlation plots comparing the overall expression profiles of each depletion against N.T. control. Heatmap number and colors indicate correlation coefficient. Topography plots show the distribution of expression changes for all genes between any two depletions within their relative contribution to the model. F. Gene ontology analysis of significantly upregulated and downregulated DEGs.

215 **Gene expression modules influenced by ASD-linked transcriptional regulators**

216

217 Next, we sought to expand these comparisons using more sensitive measures. We
218 therefore used weighted gene co-expression network analysis (WGCNA) (Zhang and Horvath
219 2005) to capture system-level changes associated with depletion of ASD-linked transcriptional
220 regulators. We found multiple gene expression modules that were significantly associated with
221 individual ASD-linked transcriptional regulators, as well as modules shared amongst multiple
222 regulators (**Fig. 4A**, **S4A, supplemental data table 5**). In particular, we detected multiple
223 significant modules enriched for genes involved in synapse function and neuronal development,
224 similar to our other analyses (**Fig 4B-C**). Interesting, we also detected gene modules linked to
225 metabolism (**Fig 4D, S4B**), another major cellular function previously linked to ASD (Rossignol
226 and Frye 2012a, 2012b). This suggests that this analysis may reveal more subtle gene
227 expression changes that also contribute to cellular changes associated with ASD. These
228 findings support the broader conclusion that ASD-linked genes have similar functional outcomes
229 rooted in transcriptional signatures that are share between conditions. Further, these different
230 analyses reveal common trends observed in ASD research more broadly including disruption of
231 neuronal synapses, neuronal development and metabolism.

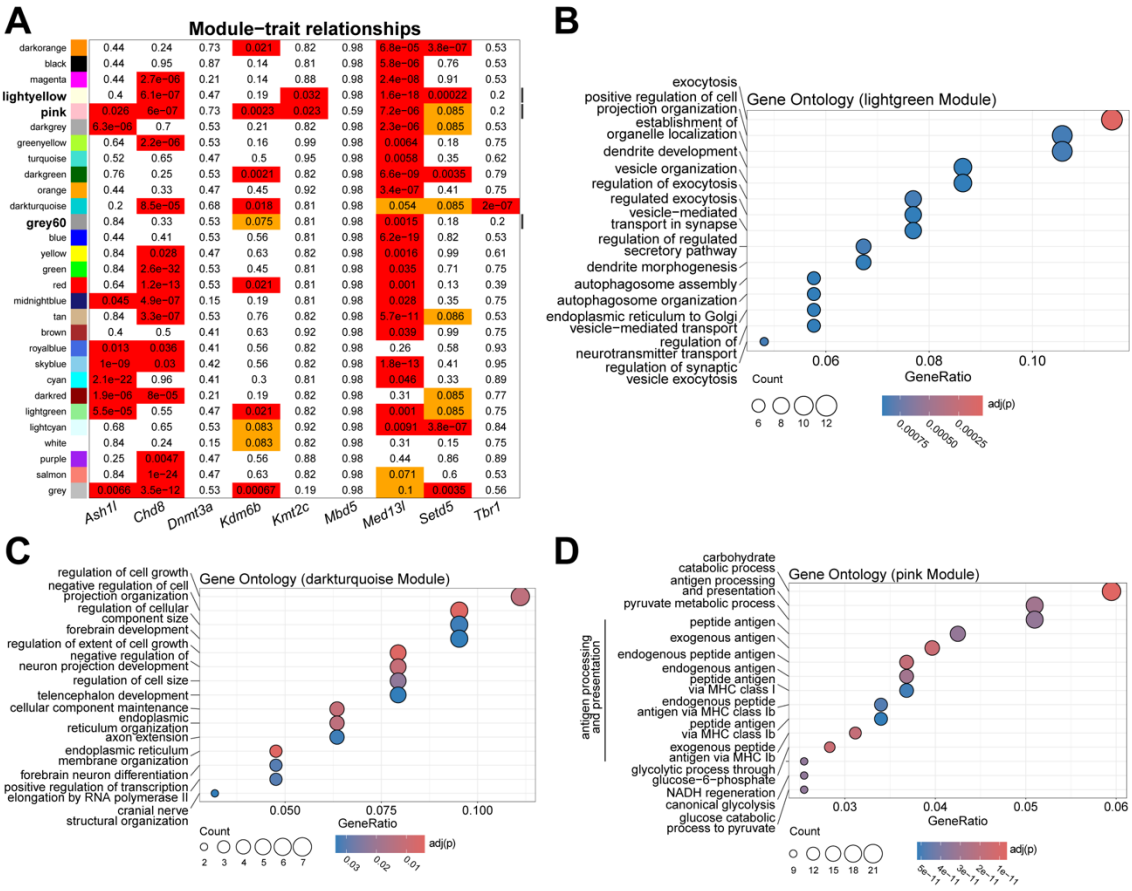

Figure 4: Shared and unique gene modules between ASD linked genes. A. WGCNA modules identified after the co-expression network construction. Numbers are the Benjamini-Hochberg corrected p values for each depletion on module expression compared to the non-targeting control with a linear model. B-D. Gene ontology analysis of shared modules. Counts indicates the number of genes in the GO term.

ASD-risk transcriptional regulators disrupt neuronal firing patterns

We consistently observe considerable disruptions to synaptic gene expression following depletion of both chromatin and transcriptional regulators linked to ASD including in studies that focused on other ASD-linked proteins (Thudium et al. 2022). We therefore asked whether these disruptions resulted in functional changes in neuronal firing patterns. To test this, we used MEA to record spontaneous firing activity of neurons depleted for each transcriptional regulator individually (**Fig. 5A, supplemental data tables 6-9**). We began testing at 12 days in culture when spiking activity low but detectable and continued through 22 days in culture. During this

period, we detected no changes in covered electrodes or resistance suggesting neurons remained healthy throughout the assay (**Fig. S5A-B**).

We found that disruption of every ASD-linked transcriptional regulator tested caused robust changes in firing patterns with decreased spike number over multiple developmental time points (**Fig. 5B**). Notably, while control neurons show anticipated increases in spiking with maturity, depletion of nearly every transcriptional regulator dampened or fully blocked this increase with maturation. In addition, we observed decreased bursting and burst duration for multiple transcriptional regulators (**Fig. 5C-D**). Even where bursting was observed, regularity of bursting was also severely disrupted (**Fig. S5C**). These data provide evidence that multiple transcriptional regulators linked to ASD are capable of severely disrupting neuronal firing and that the disruptions to synaptic gene expression detected via RNA-sequencing (**Figs. 2, 3**) result in robust functional changes. Further, we observe these effects regardless of the target examined and its specific function in regulating chromatin or transcription. These data therefore provide evidence of convergent functional effects, even with differences in target gene number and the extent of transcriptional disruptions measured.

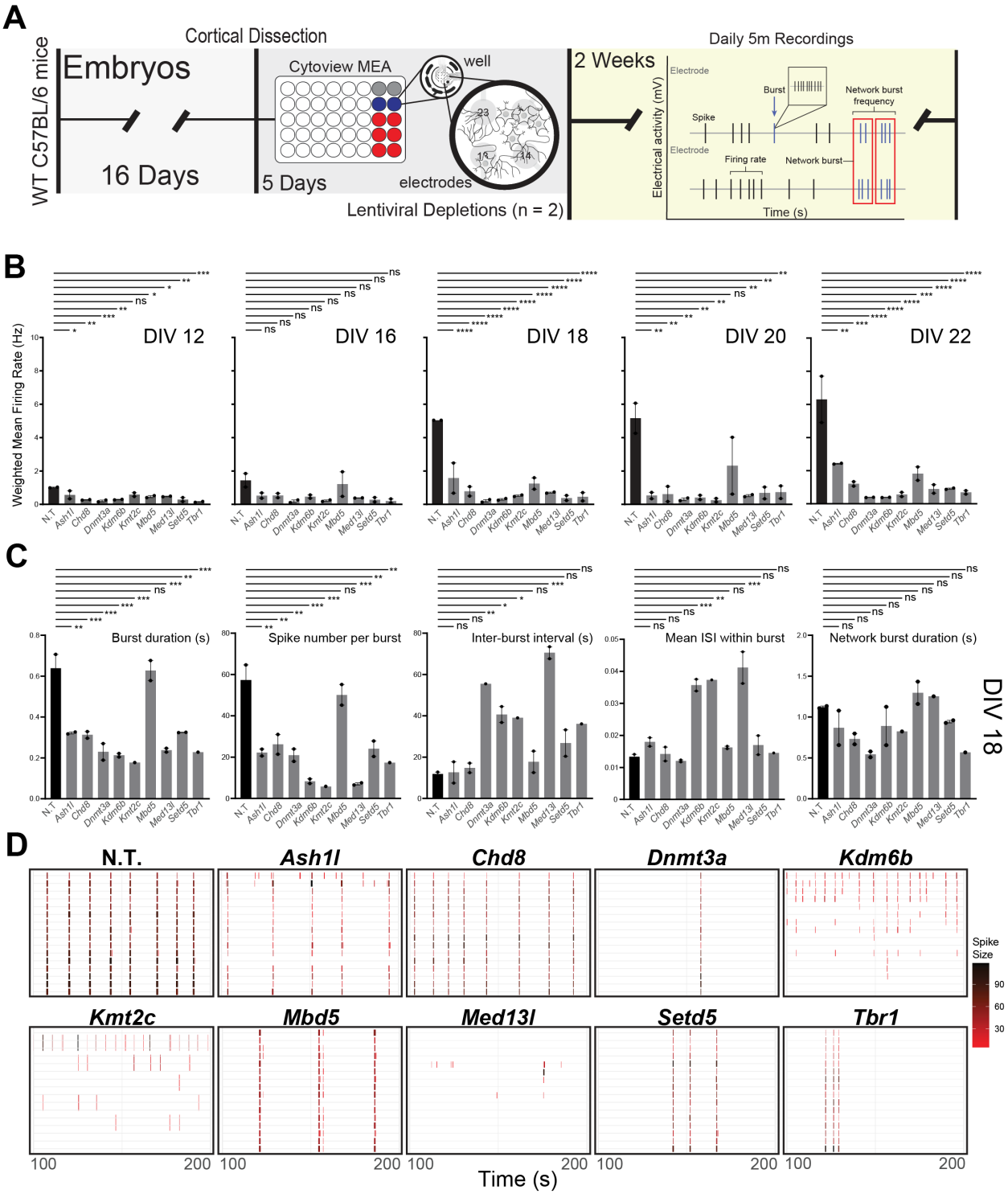

Figure 5: Changes in spontaneous firing activity due to transcriptional regulator depletion. A. Experimental timeline and schematic for the culturing and measurements of primary neurons using the multielectrode array (MEA). The recording diagram illustrates the different metrics collected by the MEA instrument. B. Weighted firing rate of each condition based only on electrodes with activity greater than the minimum spike rate from day in vitro (DIV) 12 to 22. C. Evoked metrics for each condition at DIV 18. Significance based on one-way ANOVA followed by dunnet post-test. *** ≤ 0.001, ** ≤ 0.01, * ≤ 0.05, NS = not significant. D. Example spiking patterns over the 5 minute (300 second) recording period. Two well replicates are shown for each condition.

Discussion

Here, we examined the effects of multiple ASD-linked transcriptional regulators that work through distinct mechanisms in regulating DNA, chromatin, and transcriptional output. We found that despite divergent functions, they converge on similar gene sets and their loss results in a common transcriptional signature identified through multiple analyses. This signature encodes synaptic proteins suggesting similar functional outcomes of these transcriptional disruptions. Fitting with this, we found that all tested ASD-linked genes disrupt neuronal firing and bursting patterns during neuronal maturation.

This work expanded upon prior findings by testing transcriptional regulators broadly rather than just focusing on single ASD-linked genes or only on proteins that directly modify chromatin. Instead, we selected proteins with highly divergent effects on chromatin and transcription. These included chromatin modifying enzymes that target different histone sites, chromatin remodelers from different complexes, a DNA modifying enzyme, a transcription factor, and a non-catalytic chromatin-complex protein. Even with this expanded group, we successfully identified both shared gene signature and common neuronal spiking and bursting patterns. This suggests that specific neuronal gene sets are particularly sensitive to multiple types of epigenetic manipulations and that disruption of these genes causes robust functional changes in neuronal firing.

Both the analyses overlapping individual depletion DEGs and the limma model identified several significantly downregulated genes that may be important points of convergence in the shared roles of the modifiers in affecting neuronal functioning. Topoisomerase IIα (Top2a) was downregulated in 7 of the 9 depletions in addition to being identified in the limma model. Loss of Top2a inhibits was found to inhibit the self-renewal of human neural stem cells (Qin et al. 2022) and cause social deficits in mice and zebrafish (Geng et al. 2022). Additionally, both analyses identified numerous genes important in brain development including Insulin-like growth factor 1

285 and 2 (Igf1/2) and Neuronal PAS Domain Protein 1 (Npas1). Interestingly, we also observed
286 consistent reduction in two aquaporins (Aqp4 and Aqp11) that are less well studied but also
287 linked to social and anxiety-like behavior in animal models (Davoudi et al. 2023). Together with
288 the overall reductions found in the expression data by GSEA and the functional results of the
289 MEA, these findings support the convergent roles of these chromatin modifiers on neuronal
290 biology that may contribute to neurodevelopmental disorders. WGCNA analysis similarly
291 identified several relevant modules including those enriched for genes involved in cellular
292 respiration and metabolism. Notably, metabolic dysfunction is also linked with ASD (Rossignol
293 and Frye 2012a, 2012b) and may contribute to neuronal aberrations in the disorder due to the
294 high energy demands of neurons.

295 While we identified numerous genes of interest, the system used here also has several
296 limitations. The signatures we defined are likely to be somewhat specific to the developmental
297 time selected and the model chosen. We expect that if these assays were performed at different
298 developmental time points, we would detect different gene expression signatures that may have
299 very distinct effects on functional outcomes. We thus view these results as primarily indicative of
300 sensitive genes during this stage of neuronal maturation rather than an absolute list of
301 transcriptional targets for any given gene studied here. In addition, it is likely that results will at
302 least partly diverge from human systems such as iPSC derived neurons that may more closely
303 match human developmental trajectories. Nonetheless, we view this system as offering unique
304 insights that emerge from the ability to test multiple ASD risk gene in parallel in a highly
305 controlled system with genetically identical biological replicates.

306 Together our findings demonstrate shared gene expression signatures and functional
307 outcomes of disruption of multiple ASD-linked transcriptional regulators. This work provides
308 insights into underlying cellular mechanisms that link ASD-risk genes to neuronal function and
309 highlight common pathways that are controlled by ASD-linked transcriptional regulators.

310

311 **Declaration of Interests:** The authors have no conflicts of interest.

312

313 **Acknowledgments**

314

315 Research and E.K were supported by NIH NIMH (1DP2MH129985) and NIH NINDS
316 (R01NS134755), Autism Spectrum Program of Excellence at the University of Pennsylvania
317 (ASPE), and the Eagles Autism Foundation. A.P. was supported by NIH grant T32-ES019851.
318 JEPC was supported by NIH NIMH (1R01MH120269; 1DP1MH129957); NIH NINDS (5-R01-
319 NS114226). S.S. was supported by University of Pennsylvania CURF grants. S.Z. was
320 supported by the University of Pennsylvania Epigenetics Institute. We acknowledge the use of
321 micro-electrode array equipment purchased through use of a NIH Shared
322 Equipment Grant (1S10OD032363 to J.E.P-C and E.K.).

323

324 **Methods**

325

326 Mice:
327 All mice used were on the C57BL/6J background, housed in a 12 hour light–dark cycle, and fed
328 a standard diet. All experiments were conducted in accordance with and approval of the IUCAC.

329

330 Primary Neuronal Culture:
331 Cortices were dissected from E16.5 C57BL/6J embryos and cultured in supplemented
332 neurobasal medium (Neurobasal [Gibco 21103-049], B27 [Gibco 17504044], GlutaMAX [Gibco
333 35050- 061], Pen-Strep [Gibco 15140-122]) in TC-treated 12 or 24 well plates coated with 0.05
334 mg/mL Poly-D-lysine (Sigma-Aldrich A-003-E). At 3-4 DIV, neurons were treated with 0.5 mM
335 AraC. For all experiments using cultured cortical neurons, neurons were treated with lentivirus
336 containing shRNA on DIV 5. For RNA and Protein analysis cells were collected at DIV 10.

337

338 Virus Generation and validation:

339 HEK293T cells were cultured in high-glucose DMEM growth medium (Corning 10-013-CV), 10%
340 FBS (Sigma-Aldrich F2442-500ML), and 1% Pen-Strep (Gibco 15140-122). Calcium phosphate
341 transfection was performed with Pax2 and VSVG packaging plasmids in serum-free media.
342 shRNAs in a pLKO.1-puro backbone were purchased from the Sigma-Aldrich Mission shRNA
343 library (SHCLNG) and shown in **Supplemental Table 10**. Media was changed 2h after
344 transfection and viruses were collected 24 and 48hr later. Viral media was passed through a
345 0.45-µm filter and precipitated overnight with PEG-it solution (40% PEG-8000 [Sigma-Aldrich
346 P2139-1KG], 1.2 M NaCl [Fisher Chemical S271-1]). Viral particles were pelleted at 1500g,
347 washed, and resuspended in 200 µL PBS. Virus Validation was done on E16.5 WT cortical
348 neurons. Neurons were infected with virus on DIV 5. Depletion efficiency was measured using
349 RT-qPCR with shRNA targeting luciferase as a non-targeting control.
350
351 Western:
352 After DIV 10, neurons were lysed in RIPA (25 mM Tris at pH 7.6, 150 mM NaCl, 1% NP-40, 1%
353 sodium deoxycholate, 0.1% SDS) supplemented by protease inhibitor (Roche 04693124001),
354 phosphatase inhibitor (Roche 04906837001), 1mM DTT, 1mM PMSF. Lysates were mixed with
355 5X Loading Buffer (5% SDS, 0.3 M Tris pH 6.8, 1.1 mM Bromophenol blue, 37.5% glycerol),
356 boiled for 10 minutes, sonicated for 10 minutes, and cooled on ice. Protein was resolved by 4–
357 20% Tris-glycine or 3–8% Tris-acetate SDS-PAGE (invitrogen novex gels XP04205, EA03785)
358 followed by transfer to a 0.45-µm PVDF membrane (Sigma-Aldrich IPVH00010) for
359 immunoblotting. Membranes were blocked for 1 hour in 1-5% BSA or 5% milk in TBST and
360 probed with primary antibody overnight at 4C. Antibodies are shown in **Supplemental Table 11**.
361
362 RNA Isolation:
363 Total RNA was collected from all cultures at DIV 10 using the Zymo Quick-RNA microprep kit
364 (R1050).
365

366 RT-qPCR:

367 250ng of RNA per sample was used to prepare cDNA using the high-capacity cDNA reverse
368 transcription kit (Applied Biosystems 4368813), and quantitative PCR was performed with
369 Power SYBR Green PCR master mix (Applied Biosystems 4367659). Primers are shown in
370 **Supplemental Table 12**.

371

372 RNA-seq Library Preparation:

373 Sequencing libraries were prepared using the TruSeq Stranded mRNA kit (Illumina 20040534).
374 Prior to sequencing, library size distribution was confirmed by capillary electrophoresis using an
375 Agilent 4200 TapeStation with high sensitivity D1000 reagents (5067-5585), and libraries were
376 quantified by qPCR using a KAPA Library Quantification Kit (Roche 07960140001). Libraries
377 were sequenced on an Illumina NextSeq1000 instrument (100-bp read length, paired end).

378

379 Data Processing and Differential Gene Expression:

380 Reads were mapped to Mus musculus genome build mm10 with STAR(Dobin et al. 2013)
381 (v2.7.1a) and assigned to exonic features using the featureCounts function of subRead (v2.0.3).
382 DESeq2(Love et al. 2014) (v1.38.0) was used for pairwise differential gene expression analysis
383 using a negative binomial model with default model fitting parameters. 6 WT replicates were
384 used for downstream analysis for each condition. Batch effects introduced by differences in the
385 sexes were regressed using a negative binomial model via ComBat-ref (Zhang 2024).
386 Subsetting filters were applied to determine significant DEGs as follows: baseMean of
387 normalized counts > 20, adjusted p value ≤ 0.05, and |fold change| ≥ 1.5 ($|\log_2(FC)| \geq 0.58$).
388 Integrated Genomics Viewer(Robinson et al. 2011) (v2.16.0.01) was used to visualize RNA-seq
389 read track that were normalized to the same total read number across all samples using
390 Samtools. Multifactor gene expression analysis was performed using limma (v3.52.4) via
391 edgeR(Robinson et al. 2010) (v3.38.4). Normalization factors were calculated, and expression

values were transformed to logCPM using voom(Law et al. 2014b). An empirical Bayesian distribution was calculated with weighting from all 9 depletion conditions across all samples.

Downstream Analysis:

Hypergeometric testing of significant overlaps between gene lists was performed using the dhyper density distribution without replacement using a background size of 13713 and Bonferroni correction for multiple testing. gProfiler2(Kolberg et al. 2020) (v0.2.3) was used for gene ontology analysis with g:SCS correction of multiple testing, a background list of all genes expressed in the neuronal culture (base mean of normalized counts > 20), and a term size limit of 2000 genes. SynGO was performed using the web client(Koopmans et al. 2019) (v1.2). Gene set enrichment analysis was performed using fGSEA(Korotkevich et al. 2016) (v1.22.0). This utilized a multilevel Monte Carlo approach with default parameters. Gene lists were from REACTOME or SynGO synapse umbrella terms. ChromHMM(Ernst and Kellis 2017) analysis used validated ChIP-seq data from E12.5 mouse forebrain tissue against 500bp windows directly upstream of query genes. Transcription factor motif analysis on 5kb windows directly upstream of query genes were analyzed using sequence enrichment analysis in the MEME suite(Bailey and Grant 2021) (v5.5.7). Motifs were scanned using the JASPAR 2020 Core Vertebrates database using the windows 5kb upstream of 1000 randomly selected genes expressed in neurons. WGCNA was used to construct a signed co-expression network(Langfelder and Horvath 2008) (v1.73). Batch-corrected inputs were filtered for those with read count ≥ 10 and normalized using variance stabilizing transformation of DESeq2 with design = ~ depletion. Network construction used a soft threshold blcokSize = 20000, networkType = “Signed”, power of 20, scale free topology fit of 0.83, and minimum module size of 40. For each module, we calculated its expression (ME, module eigengene) as the first principal component of normalized expression. We used a linear model to test the effect of each depletion on module expression compared to non-targeting control. P values were corrected using Benjamini-Hochberg correction. Gene ontology for WGCNA was performed using the

419 enrichGO function from clusterProfiler(Yu et al. 2012) (v4.10.1) with the BP ontology database,
420 Benjamini-Hochberg correction, p value cutoff of 0.05, and q value cutoff of 0.05. The top 15
421 terms per analysis were selected for figures.
422
423 MEA Analysis:
424 Primary neuronal culturing was performed as described above using E16.5 embryos derived
425 from mating of Female mice (C57BL/6N). Cerebral cortices were isolated from two pups from
426 two separate litters and dissociated as described above, then plated in poly-D-lysine/laminin-
427 coated multielectrode array plates (M768-tMEA-48W, Axion Biosystems) using the dot plate
428 method, at 70K cells/well. For viral infections, each well was uniquely infected with one of the 9
429 ASD targets or non-targeting shRNA at DIV 5. Viral media was removed after 20 hr of exposure
430 and replaced with enriched neurobasal media. After 11 days, the synaptic activity of cultured
431 neurons was recorded daily using the Maestro MEA system (Axion Biosystems, Atlanta, GA,
432 USA). Recordings were done 5 and 30 minutes after placing in MEA machine at 5% CO2 and at
433 37C. Metrics were further processed using Prism with a one-way ANOVA followed by dunnet
434 post-test and R.
435
436 **Data availability**
437
438 All sequencing data are available at **GSE286067**
439 Reviewer token: opelqgcahrafpoz
440
441 **Figure legends**
442
443 **Table 1: Function and association data for the nine transcriptional regulators chosen for**
444 **analysis.** SFARI gene score of 1 indicates high confidence for implication in autism spectrum

445 disorder. Evaluation of Autism Gene Link Evidence (EAGLE) score ranges from 6 (limited) to
446 12+ (definitive) roles in autism for validated targets.
447
448 **Figure 1: Gene expression analysis of nine independent chromatin modifier depletions in**
449 **primary mouse neurons. A.** Schematic of the experimental timeline for the comparison of
450 transcriptomes between chromatin modifier depletions. **B.** Counts per million (CPM) for the nine
451 chromatin modifiers following lentivirus-mediated shRNA depletion of each target, relative to the
452 average of nontargeting (N.T.) treated neurons (n = 6). **C.** Total up or downregulated
453 differentially expressed genes (DEGs) in the pairwise comparison of each depletion versus N.T.
454 treated neurons. Full DEG lists shown in Supplemental Table 1. D-E. Gene ontology analysis of
455 significantly up and downregulated genes in the depletion of Tbr1 or Kdm6b (**D**) and Med13l (**E**).
456 Recall is the proportion of functionally annotated genes in the query over the number of genes
457 in the GO term. Precision is the number of genes found in the GO term over the total number of
458 genes in the query. Results for other targets shown in Supplemental Table 2. **F.** SynGO for
459 Med13l significantly downregulated DEGs. **G-H.** GSEA of genes in the SynGO postsynaptic
460 membrane potential (**G**) or synaptic adhesion (**H**) terms for each depletion transcriptional
461 signature. NES indicates the directional normalized enrichment score.
462
463 **Figure 2: Identifying transcripts that co-dysregulated across depletions. A.** Upset plot of
464 up or downregulated DEG found in at least two depletions. Gene placement prioritizes the
465 largest intersection possible, only showing overlaps with 3 or more DEGs. **B.** Significance of
466 overlap for up or downregulated DEGs after each depletion using hypergeometric tests. **C.**
467 Heatmap of DEGs that appear in 4+ (left, downregulated, right, upregulated) comparisons
468 between depletion and N.T. control. **D.** Gene tracks of aligned transcripts over genes that were
469 either upregulated (Myd88) or downregulated (Thbs1) in multiple depletions. **E.** Gene ontology
470 analysis of all significantly downregulated genes found in over 2 or over 3 depletion conditions.
471 **F.** Boxplots of the transcript lengths for all genes, each DEG found up or downregulated in at

472 least 2 pairwise depletions, or 3 pairwise depletions. T-test p values for each pairwise
473 comparison are noted on the side.
474
475
476 **Figure 3: Multiple factor linear modeling to determine commonly disrupted transcripts**
477 **across all nine depletions. A.** Volcano plot of DEGs from the limma/voom model factoring all
478 nine depletion conditions against N.T. control. **B.** Gene tracks of transcripts of the top 2 DEGs
479 Tmem230 and Ankrd29. **C.** Relative expression of the top DEGs identified in the multi-factor
480 model in each depletion versus the average of nontargeting (N.T.) treated neurons. **D.** Overlap
481 of genes down or upregulated in at least 2 (i) or 3 (ii) pairwise comparisons and those from the
482 multi-factor model. Hypergeometric test results for each overlap as shown in red. **E.** Cross-
483 correlation plots comparing the overall expression profiles of each depletion against N.T. control.
484 Heatmap number and colors indicate correlation coefficient. Topography plots show the
485 distribution of expression changes for all genes between any two depletions within their relative
486 contribution to the model. **F.** Gene ontology analysis of significantly upregulated and
487 downregulated DEGs.
488
489 **Figure 4: Shared and unique gene modules between ASD linked genes. A.** WGCNA
490 modules identified after the co-expression network construction. Numbers are the Benjamini-
491 Hochberg corrected p values for each depletion on module expression compared to the non-
492 targeting control with a linear model. **B-D.** Gene ontology analysis of shared modules. Counts
493 indicates the number of genes in the GO term.
494
495 **Figure 5: Changes in spontaneous firing activity due to transcriptional regulator**
496 **depletion. A.** Experimental timeline and schematic for the culturing and measurements of
497 primary neurons using the multielectrode array (MEA). The recording diagram illustrates the
498 different metrics collected by the MEA instrument. **B.** Weighted firing rate of each condition

499 based only on electrodes with activity greater than the minimum spike rate from day in vitro
500 (DIV) 12 to 22. **C.** Evoked metrics for each condition at DIV 18. Significance based on one-way
501 ANOVA followed by dunnet post-test. *** ≤ 0.001, ** ≤ 0.01, * ≤ 0.05, NS = not significant. **D.**
502 Example spiking patterns over the 5 minute (300 second) recording period. Two well replicates
503 are shown for each condition.
504
505 **Supplemental Figure 1: Validation of depletions. A.** Relative transcript expression level of
506 each chromatin modifier following depletion versus non-targeting control virus (N.T.) treated
507 neurons as measured by RT-qPCR. **B.** Western blots showing protein level of four of the
508 chromatin modifiers in control-treated and shRNA-treated neurons. **C.** Principal component
509 analysis of the pairwise comparison between neurons with no virus (N.V.) and and those treated
510 with N.T. control (n = 6, 3 female and 3 male for each condition). **D.** Volcano plot of differential
511 gene expression between no N.V. and N.T. neurons. **E.** Scatterplot of the number of DEGs
512 identified in the comparison between a depletion of a modifier and control against the average
513 expression of that modifier following depletion. **F.** Scatterplot of the number of DEGs identified in
514 the comparison between a depletion of a modifier and control against the counts per million
515 (CPM) normalized expression of that modifier.
516
517 **Supplemental Figure 2: Differential gene expression overlaps and genomic features. A.**
518 Overlap of significantly up (red) or down (blue) regulated genes in each of the individual modifier
519 depletions against the SFARI database for autism-associated genes with at least one report
520 (1141 genes). **B.** ChromHMM analysis of promoters (500bp upstream of transcription start sites,
521 TSS) of significantly up or downregulated genes found in at least one depletion, over two, or
522 over three.
523
524 **Supplemental Figure 3: Multi-factor limma model overlaps and genomic features. A.**
525 Overlap of significantly up (red) or down (blue) regulated genes in the multi-factor limma model

526 against the SFARI database for autism-associated genes with at least one report (1141 genes).
527 Hypergeometric test results for each overlap are shown in red. **B.** Boxplots of the transcript
528 lengths from the multi-factor limma model. T-test p values for each pairwise comparison are
529 noted on the side.
530
531 **Supplemental Figure 4: WGCNA analysis module gene ontology. A.** Cluster dendrogram of
532 the classification of genes to each model. **B-C.** Gene ontology analysis of additional top shared
533 modules. Note that the Grey module expression explains less than 10% of the module so was
534 not analyzed by GO while other modules expression explain > ~50% of module variation.
535
536 **Supplemental Figure 5: Multi-electrode array control metrics. A.** Number of covered
537 electrodes per well per condition as defined by those with resistance greater than the threshold
538 of 18 kΩ. **B.** Average resistance in each well across conditions from day in vitro (DIV) 12 to 22.
539 **C.** Synchrony measures for each well of each condition at DIV 18 as defined the inter-electrode
540 cross correlation across all spikes.
541
542 **Supplemental Data Table 1. Differential gene expression by depletion.**
543 **Supplemental Data Table 2. Gene ontology results by depletion.**
544 **Supplemental Data Table 3. Overlap of DEGs.**
545 **Supplemental Data Table 4. Limma voom analysis of depletions.**
546 **Supplemental Data Table 5. WGCNA modules.**
547 **Supplemental Data Table 6. MEA resistances.**
548 **Supplemental Data Table 7. MEA mean firing rates.**
549 **Supplemental Data Table 8. MEA weighted mean firing rates.**
550 **Supplemental Data Table 9. MEA bursting.**
551 **Supplemental Data Table 10. shRNA oligo sequences.**
552 **Supplemental Data Table 11. Antibodies and dilutions used.**

553 **Supplemental Data Table 12. Primer sequences.**

554

555 **References**

556 Adegbola A, Musante L, Callewaert B, Maciel P, Hu H, Isidor B, Picker-Minh S, Le Caignec C,
557 Delle Chiaie B, Vanakker O, et al. 2015. Redefining the MED13L syndrome. *Eur J Hum*
558 *Genet* **23**: 1308–1317.

559 Bailey TL, Grant CE. 2021. SEA: Simple Enrichment Analysis of motifs.
560 http://biorxiv.org/lookup/doi/10.1101/2021.08.23.457422 (Accessed January 6, 2025).

561 Beighley JS, Hudac CM, Arnett AB, Peterson JL, Gerdts J, Wallace AS, Mefford HC, Hoekzema
562 K, Turner TN, O'Roak BJ, et al. 2020. Clinical Phenotypes of Carriers of Mutations in
563 CHD8 or Its Conserved Target Genes. *Biol Psychiatry* **87**: 123–131.

564 Bernier R, Golzio C, Xiong B, Stessman HA, Coe BP, Penn O, Witherspoon K, Gerdts J, Baker
565 C, Vulto-van Silfhout AT, et al. 2014. Disruptive CHD8 mutations define a subtype of
566 autism early in development. *Cell* **158**: 263–276.

567 Brauer B, Merino-Veliz N, Ahumada-Marchant C, Arriagada G, Bustos FJ. 2023. KMT2C
568 knockout generates ASD-like behaviors in mice. *Front Cell Dev Biol* **11**: 1227723.

569 Camarena V, Cao L, Abad C, Abrams A, Toledo Y, Araki K, Araki M, Walz K, Young JI. 2014.
570 Disruption of Mbd5 in mice causes neuronal functional deficits and neurobehavioral
571 abnormalities consistent with 2q23.1 microdeletion syndrome. *EMBO Mol Med* **6**: 1003–
572 1015.

573 Chatterjee I, Getselter D, Ghaneem N, Bel S, Elliott E. 2021. *CHD8 regulates gut epithelial cell*
574 *function and affects autism-related behaviours through the gut-brain axis*. Neuroscience
575 http://biorxiv.org/lookup/doi/10.1101/2021.10.02.462735 (Accessed June 30, 2023).

576 Christian DL, Wu DY, Martin JR, Moore JR, Liu YR, Clemens AW, Nettles SA, Kirkland NM,
577 Papouin T, Hill CA, et al. 2020. DNMT3A Haploinsufficiency Results in Behavioral
578 Deficits and Global Epigenomic Dysregulation Shared across Neurodevelopmental
579 Disorders. *Cell Reports* **33**: 108416.

580 Davoudi S, Rahdar M, Hosseinmardi N, Behzadi G, Janahmadi M. 2023. Chronic inhibition of
581 astrocytic aquaporin-4 induces autistic-like behavior in control rat offspring similar to
582 maternal exposure to valproic acid. *Physiol Behav* **269**: 114286.

583 de la Torre-Ubieta L, Won H, Stein JL, Geschwind DH. 2016. Advancing the understanding of
584 autism disease mechanisms through genetics. *Nat Med* **22**: 345–361.

585 De Rubeis S, He X, Goldberg AP, Poultney CS, Samocha K, Cicek AE, Kou Y, Liu L, Fromer M,
586 Walker S, et al. 2014. Synaptic, transcriptional and chromatin genes disrupted in autism.
587 *Nature* **515**: 209–215.

588 Dobin A, Davis CA, Schlesinger F, Drenkow J, Zaleski C, Jha S, Batut P, Chaisson M, Gingeras
589 TR. 2013. STAR: ultrafast universal RNA-seq aligner. *Bioinformatics* **29**: 15–21.

590 Ernst J, Kellis M. 2017. Chromatin-state discovery and genome annotation with ChromHMM.
591 *Nat Protoc* **12**: 2478–2492.

592 Fu JM, Satterstrom FK, Peng M, Brand H, Collins RL, Dong S, Wamsley B, Klei L, Wang L, Hao
593 SP, et al. 2022. Rare coding variation provides insight into the genetic architecture and
594 phenotypic context of autism. *Nat Genet* **54**: 1320–1331.

595 Gao Y, Duque-Wilckens N, Aljazi MB, Wu Y, Moeser AJ, Mias GI, Robison AJ, He J. 2021. Loss
596 of histone methyltransferase ASH1L in the developing mouse brain causes autistic-like
597 behaviors. *Commun Biol* **4**: 1–10.

598 Geng Y, Zhang T, Alonzo IG, Godar SC, Yates C, Pluimer BR, Harrison DL, Nath AK, Yeh J-RJ,
599 Drummond IA, et al. 2022. Top2a promotes the development of social behavior via
600 PRC2 and H3K27me3. *Science Advances* **8**: eabm7069.

601 Huang T-N, Yen T-L, Qiu LR, Chuang H-C, Lerch JP, Hsueh Y-P. 2019. Haploinsufficiency of
602 autism causative gene Tbr1 impairs olfactory discrimination and neuronal activation of
603 the olfactory system in mice. *Molecular Autism* **10**: 5.

604 Hurley S, Mohan C, Suetterlin P, Ellingford R, Riegman KLH, Ellegood J, Caruso A, Michetti C,
605 Brock O, Evans R, et al. 2021. Distinct, dosage-sensitive requirements for the autism-
606 associated factor CHD8 during cortical development. *Mol Autism* **12**: 16.

607 Iossifov I, O'Roak BJ, Sanders SJ, Ronemus M, Krumm N, Levy D, Stessman HA, Witherspoon
608 KT, Vives L, Patterson KE, et al. 2014. The contribution of de novo coding mutations to
609 autism spectrum disorder. *Nature* **515**: 216–21.

610 King IF, Yandava CN, Mabb AM, Hsiao JS, Huang H-S, Pearson BL, Calabrese JM, Starmer J,
611 Parker JS, Magnuson T, et al. 2013. Topoisomerases facilitate transcription of long
612 genes linked to autism. *Nature* **501**: 58–62.

613 Kolberg L, Raudvere U, Kuzmin I, Vilo J, Peterson H. 2020. gprofiler2 -- an R package for gene
614 list functional enrichment analysis and namespace conversion toolset g:Profiler.
615 *F1000Res* **9**: ELIXIR-709.

616 Koopmans F, van Nierop P, Andres-Alonso M, Byrnes A, Cijsouw T, Coba MP, Cornelisse LN,
617 Farrell RJ, Goldschmidt HL, Howrigan DP, et al. 2019. SynGO: An Evidence-Based,
618 Expert-Curated Knowledge Base for the Synapse. *Neuron* **103**: 217-234.e4.

619 Korotkevich G, Sukhov V, Budin N, Shpak B, Artyomov MN, Sergushichev A. 2016. Fast gene
620 set enrichment analysis. http://biorxiv.org/lookup/doi/10.1101/060012 (Accessed January
621 6, 2025).

622 Langfelder P, Horvath S. 2008. WGCNA: an R package for weighted correlation network
623 analysis. *BMC Bioinformatics* **9**: 559.

624 Lavery WJ, Barski A, Wiley S, Schorry EK, Lindsley AW. 2020. KMT2C/D COMPASS complex-
625 associated diseases [KCDCOM-ADs]: an emerging class of congenital regulopathies.
626 *Clin Epigenetics* **12**: 10.

627 Law CW, Chen Y, Shi W, Smyth GK. 2014a. voom: precision weights unlock linear model
628 analysis tools for RNA-seq read counts. *Genome Biology* **15**: R29.

Law CW, Chen Y, Shi W, Smyth GK. 2014b. voom: Precision weights unlock linear model analysis tools for RNA-seq read counts. *Genome Biol* **15**: R29.

Li J, Pinto-Duarte A, Zander M, Cuoco MS, Lai C-Y, Osteen J, Fang L, Luo C, Lucero JD, Gomez-Castanon R, et al. Dnmt3a knockout in excitatory neurons impairs postnatal synapse maturation and increases the repressive histone modification H3K27me3. *eLife* **11**: e66909.

Love MI, Huber W, Anders S. 2014. Moderated estimation of fold change and dispersion for RNA-seq data with DESeq2. *Genome Biol* **15**: 550.

Moore SM, Seidman JS, Ellegood J, Gao R, Savchenko A, Troutman TD, Abe Y, Stender J, Lee D, Wang S, et al. 2019. Setd5 haploinsufficiency alters neuronal network connectivity and leads to autistic-like behaviors in mice. *Transl Psychiatry* **9**: 24.

Mullegama SV, Elsea SH. 2016. Clinical and Molecular Aspects of MBD5-Associated Neurodevelopmental Disorder (MAND). *Eur J Hum Genet* **24**: 1376.

Nakamura T, Yoshihara T, Tanegashima C, Kadota M, Kobayashi Y, Honda K, Ishiwata M, Ueda J, Hara T, Nakanishi M, et al. 2024. Transcriptomic dysregulation and autistic-like behaviors in Kmt2c haploinsufficient mice rescued by an LSD1 inhibitor. *Mol Psychiatry* 1–17.

O'Roak BJ, Vives L, Girirajan S, Karakoc E, Krumm N, Coe BP, Levy R, Ko A, Lee C, Smith JD, et al. 2012. Sporadic autism exomes reveal a highly interconnected protein network of de novo mutations. *Nature* **485**: 246–250.

Parikshak NN, Luo R, Zhang A, Won H, Lowe JK, Chandran V, Horvath S, Geschwind DH. 2013. Integrative functional genomic analyses implicate specific molecular pathways and circuits in autism. *Cell* **155**: 1008–1021.

Qin S, Yuan Y, Huang X, Tan Z, Hu X, Liu H, Pu Y, Ding Y, Su Z, He C. 2022. Topoisomerase IIA in adult NSCs regulates SVZ neurogenesis by transcriptional activation of Usp37. *Nucleic Acids Research* **50**: 9319–9338.

Rajarajan P, Borrman T, Liao W, Schrode N, Flaherty E, Casiño C, Powell S, Yashaswini C, LaMarca EA, Kassim B, et al. 2018. Neuron-specific signatures in the chromosomal connectome associated with schizophrenia risk. *Science* **362**: eaat4311.

Ritchie ME, Phipson B, Wu D, Hu Y, Law CW, Shi W, Smyth GK. 2015. limma powers differential expression analyses for RNA-sequencing and microarray studies. *Nucleic Acids Research* **43**: e47.

Robinson JT, Thorvaldsdóttir H, Winckler W, Guttman M, Lander ES, Getz G, Mesirov JP. 2011. Integrative genomics viewer. *Nat Biotechnol* **29**: 24–26.

Robinson MD, McCarthy DJ, Smyth GK. 2010. edgeR: a Bioconductor package for differential expression analysis of digital gene expression data. *Bioinformatics* **26**: 139–140.

Rossignol DA, Frye RE. 2012a. A review of research trends in physiological abnormalities in autism spectrum disorders: immune dysregulation, inflammation, oxidative stress, mitochondrial dysfunction and environmental toxicant exposures. *Mol Psychiatry* **17**: 389–401.

669 Rossignol DA, Frye RE. 2012b. Mitochondrial dysfunction in autism spectrum disorders: a
670 systematic review and meta-analysis. *Mol Psychiatry* **17**: 290–314.

671 Satterstrom FK, Kosmicki JA, Wang J, Breen MS, Rubeis SD, An J-Y, Peng M, Collins R, Grove
672 J, Klei L, et al. 2020. Large-Scale Exome Sequencing Study Implicates Both
673 Developmental and Functional Changes in the Neurobiology of Autism. *Cell* **180**: 568-
674 584.e23.

675 Schrode N, Ho S-M, Yamamuro K, Dobbyn A, Huckins L, Matos MR, Cheng E, Deans PJM,
676 Flaherty E, Barretto N, et al. 2019. Synergistic effects of common schizophrenia risk
677 variants. *Nat Genet* **51**: 1475–1485.

678 Shen W, Krautscheid P, Rutz AM, Bayrak-Toydemir P, Dugan SL. 2019. De novo loss-of-function
679 variants of ASH1L are associated with an emergent neurodevelopmental disorder. *Eur J*
680 *Med Genet* **62**: 55–60.

681 Sullivan PF, Geschwind DH. 2019. Defining the Genetic, Genomic, Cellular, and Diagnostic
682 Architectures of Psychiatric Disorders. *Cell* **177**: 162–183.

683 Thudium S, Palozola K, L'Her É, Korb E. 2022. Identification of a transcriptional signature found
684 in multiple models of ASD and related disorders. *Genome Res*.

685 Yu G, Wang L-G, Han Y, He Q-Y. 2012. clusterProfiler: an R package for comparing biological
686 themes among gene clusters. *OMICS* **16**: 284–287.

687 Zhang B, Horvath S. 2005. A general framework for weighted gene co-expression network
688 analysis. *Stat Appl Genet Mol Biol* **4**: Article17.

689 Zhang X. 2024. Highly effective batch effect correction method for RNA-seq count data. *Comput*
690 *Struct Biotechnol J* **27**: 58–64.

691 Zhao Y-T, Kwon DY, Johnson BS, Fasolino M, Lamonica JM, Kim YJ, Zhao BS, He C, Vahedi G,
692 Kim TH, et al. 2018. Long genes linked to autism spectrum disorders harbor broad
693 enhancer-like chromatin domains. *Genome Res* **28**: 933–942.

694